Journal of
Micro/Nanolithography, MEMS, and MOEMS

Nanolithography.SPIEDigitalLibrary.org

Observation of phase defect on extreme ultraviolet mask using an extreme ultraviolet microscope

Tsuyoshi Amano
Tsuneo Terasawa
Hidehiro Watanabe
Mitsunori Toyoda
Tetsuo Harada
Takeo Watanabe
Hiroo Kinoshita

SPIE.

Observation of phase defect on extreme ultraviolet mask using an extreme ultraviolet microscope

Tsuyoshi Amano,[a,*] Tsuneo Terasawa,[a] Hidehiro Watanabe,[a] Mitsunori Toyoda,[b] Tetsuo Harada,[c] Takeo Watanabe,[c] and Hiroo Kinoshita[c]
[a]EUVL Infrastructure Development Center, Inc., 16-1 Onogawa, Tsukuba, Ibaraki 305-8569, Japan
[b]Tohoku University, Laboratory of Soft X-ray Microscopy, Katahira, Aoba, Sendai, Miyagi 980-8577, Japan
[c]University of Hyogo, Center for EUV Lithography, LASTI, Kamigori, Hyogo 678-1205, Japan

Abstract. Influences of phase defect structures on extreme ultraviolet (EUV) microscope images were examined. Phase defects on the bottom of a multilayer (ML) do not always propagate vertically upward to the ML's top surface. For this study, two types of masks were prepared. One was an EUV blank with programmed phase defects made of lines in order to analyze the inclination angle of the phase defects. The other was an EUV mask that consists of programmed dot type phase defects 80 nm wide and 2.4 nm high with absorber patterns of half-pitch 88-nm lines-and-spaces. The positions of the phase defects relative to the absorber lines were designed to be shifted accordingly. Transmission electron microscope observations revealed that the line type phase defects starting from the bottom surface of the ML propagated toward the ML's top surface, while inclined toward the center of the EUV blank. At the distances of 0 and 66 mm from the center of the EUV blank, the inclination angles varied from 0 to 4 deg. The impacts of the inclination angles on EUV microscope images were significant even though the positions of the phase defect relative to the absorber line, as measured by a scanning probe microscope, were the same. © *The Authors. Published by SPIE under a Creative Commons Attribution 3.0 Unported License. Distribution or reproduction of this work in whole or in part requires full attribution of the original publication, including its DOI.* [DOI: 10.1117/1.JMM.13.2.023012]

Keywords: extreme ultraviolet; extreme ultraviolet microscope; phase defect; defect mitigation; compensation repair.

Paper 14034P received Mar. 26, 2014; revised manuscript received May 22, 2014; accepted for publication May 28, 2014; published online Jun. 24, 2014.

1 Introduction

Extreme ultraviolet (EUV) lithography is considered to be the most promising next-generation lithography after the point where 193-nm immersion lithography would cease to deliver smaller features. However, the path toward establishing the EUV lithography faces many technical difficulties. Issues with insufficient light-source power, particle-free mask handling, defect-free mask, availability of flat mask blanks,[1–5] and resist material development[6,7] are some of those difficulties that need to be resolved. From the viewpoint of EUV mask fabrication, mask pattern defect inspection[8–10] and repair[11–13] are some of the even more demanding tasks to be addressed. The reason is that for the EUV lithography generation, the device pattern feature size happens to be exceedingly small and calls for higher repairing accuracy than what has been achieved for optical lithography.[14–16] Regarding the types of defects, the nature of the pattern defects in the EUV mask is mostly the same as in the case of optical masks except for those defects that are classified as reflective multilayer (ML) defects, such as bump or pit phase defects that propagate through the ML during their deposition, and are hard to repair.[17] Therefore, to minimize the effect of the phase defect on the printed images on wafer, two methods are suggested. One method is to cover the phase defects beneath the absorber pattern by shifting the location of the device pattern during the mask patterning.[18–20] The other is to eliminate the influence of the phase error by simply removing the absorber away from the close proximity of the phase defects after fabricating the device pattern.[21] To make these methods succeed, it would be necessary to be able to pinpoint the locations of the phase defects and the affected areas.[22–24]

As for the growth model of the phase defect due to the bumps on the quartz substrate surface, several transmission electron microscope (TEM) images of the phase defects indicated that the growth of a phase defect starting as a bump on the quartz substrate surface does not always propagate in a vertical direction.[25,26] This means that ML surface geometry measurement of phase defects using scanning probe microscope (SPM) or nonactinic system may not be the right tool for phase defect mitigation strategy of covering, or compensating for, the phase defects by manipulating the absorber pattern. Therefore, to understand the influence of the propagation angle of the phase defect on the compensation strategy, a programmed phase defect EUV mask was prepared, and absorber lines with the phase defects were observed using SPM and EUV microscope.

2 Experiment

2.1 *Preparation of a Programmed Line Type Phase Defect EUV Blank*

A programmed line type phase defect EUV blank (with no absorber) consists of a Ru-capped Mo/Si ML deposited on a quartz substrate with seeds on quartz for the creation of line type phase defects. The ML consisted of a 2.5-nm-thick Ru film on a 40-bilayer Mo (2.2 nm thick)/Si (4.8 nm thick) film. To serve as seeds for the phase defects, lines of 100 nm in width, arrayed in 7×7 with a pitch of 22 mm, were fabricated on the quartz substrate. As a first step, a

*Address all correspondence to: Tsuyoshi Amano, E-mail: tsuyoshi.amano@eidec.co.jp

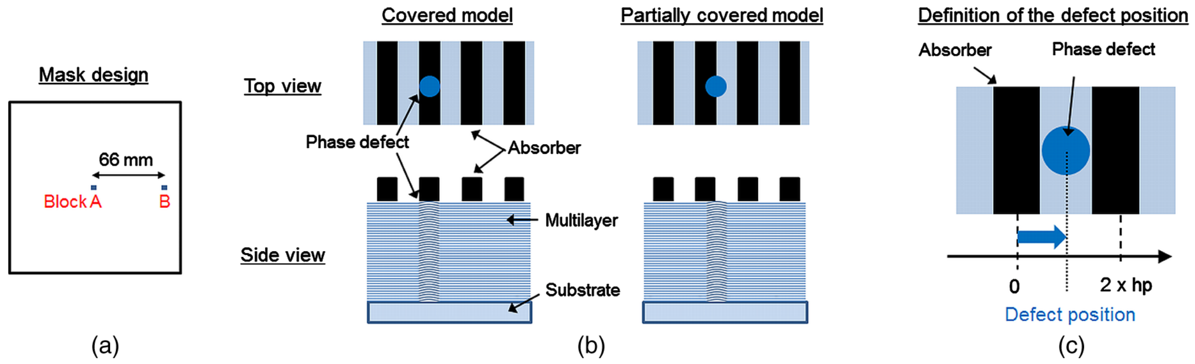

Fig. 1 (a) Arrangement of the test pattern. (b) Illustrations of the hp 88-nm L/S pattern with dot type phase defect. (c) Definition of the phase defect position.

photoresist layer was coated on the chrome layer on a quartz substrate. Next, a set of line patterns were drawn on the photoresist layer by an electron beam writing system (EBM-8000, NuFlare Technology Inc., Yokohama, Japan). Then after developing the photoresist layer, the chrome layer was etched. As a last step, the quartz substrate was etched and the chrome layer was removed. After running through a cleaning process, the patterned substrate was then coated with a Ru-capped ML. The nonflatness of the blank before and after the ML coating was below 20 and 800 nm, respectively, and the ML surface was higher in the center of the EUV blank than in its corners.

2.2 *Preparation of a Programmed Dot Type Phase Defect EUV Mask*

To investigate the influence of the phase defect on EUV microscope images, a programmed phase defect EUV mask was prepared. Figure 1(a) shows the mask design. Dots on quartz substrate and the absorber patterns of half-pitch (hp) 88-nm L/S were arrayed in block A (at the center of the mask) and block B (66 mm away from the block A). The fabrication processes of the dot type phase defects are same as the line type phase defects. The positions of the phase defects relative to the absorber lines were designed to be shifted in a prescribed fashion as shown in Fig. 1(b). The position of the phase defect was defined as 0 nm when the center of the phase defect coincided with the center of the absorber line. The right side of the absorber line was defined as plus direction as shown in Fig. 1(c). The dimensions and the positions of the phase defects at the mask surface were measured using an SPM (L-Trace II, Hitachi High-Tech Science Corp., Tokyo, Japan).

2.3 *Imaging Conditions and Data Analysis*

Figure 2 illustrates the imaging optics of the EUV microscope developed by Tohoku University[27] that was utilized in this study. The EUV light was sourced from a beam line BL3 of the NewSUBARU synchrotron facility at the University of Hyogo. The outer and inner numerical apertures of the illumination optics were 0.25 and 0.14, respectively. The coherence factor of the illumination light was about 0.01 because the synchrotron source size is very low. The incident angle of the EUV light to the EUV mask was 11 deg, and the angle between the plane of incidence and line pattern direction was approximately 20 deg. The exposure time to take an image was set at 30 s. To reduce the influence of the speckle noise on the EUV microscope image, nine images of the same pattern were taken and superimposed.

Figures 3(a) and 3(b) show the schematic models of an EUV mask and an EUV microscope image of the mask, respectively. When a phase defect is not adequately covered by the absorber line, image intensity of the L/S pattern varies depending on the phase defect position. Figure 3(c) shows the intensity profile of the EUV microscope image along a line A-A′ drawn across the L/S pattern containing the defect. Here, I_{ML}, I_{ABS}, and I_{DEF} stand for the intensities of the reflected lights from the space pattern without the phase defect, line pattern, and space pattern with the phase defect, respectively. The normalized intensity was calculated by the following equations:

$$I = (I_{\mathrm{DEF}} - I_{\mathrm{ABS}})/(I_{\mathrm{ML}} - I_{\mathrm{ABS}}). \tag{1}$$

3 Results and Discussions

3.1 *Analysis of the Phase Defect Structure*

According to our previous work, the path of a pit type phase defect propagating from the bottom of an ML and ending at the top is inclined toward the center of the mask.[28] Furthermore, the inclination angle increases in proportion to the distance from the center of the mask. In this section, to determine the increasing angle of inclination, and to

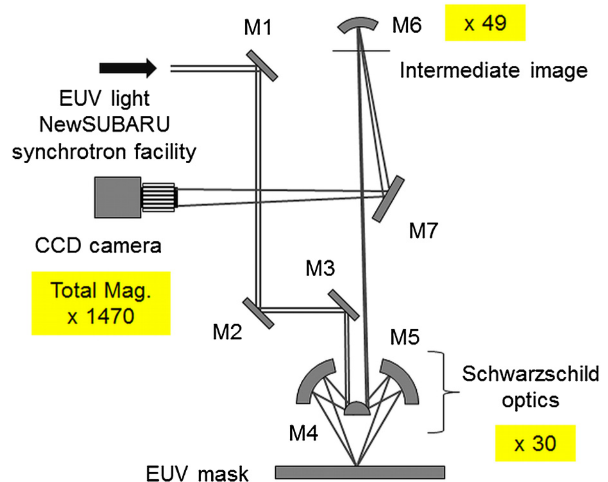

Fig. 2 Schematic model of the extreme ultraviolet (EUV) microscope optics.

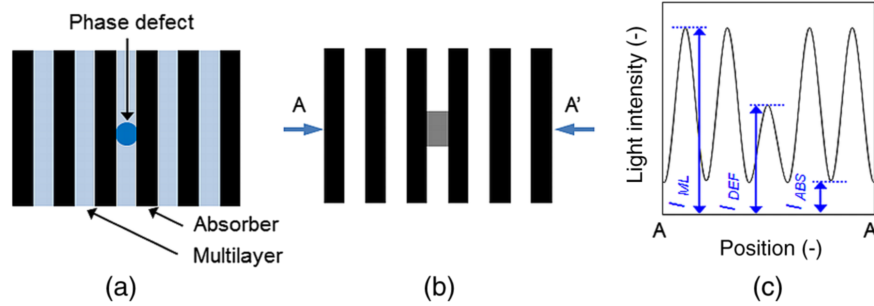

Fig. 3 Illustrations of (a) the phase defect in L/S pattern and (b) the EUV microscope image. (c) Intensity profiles along the line AA′.

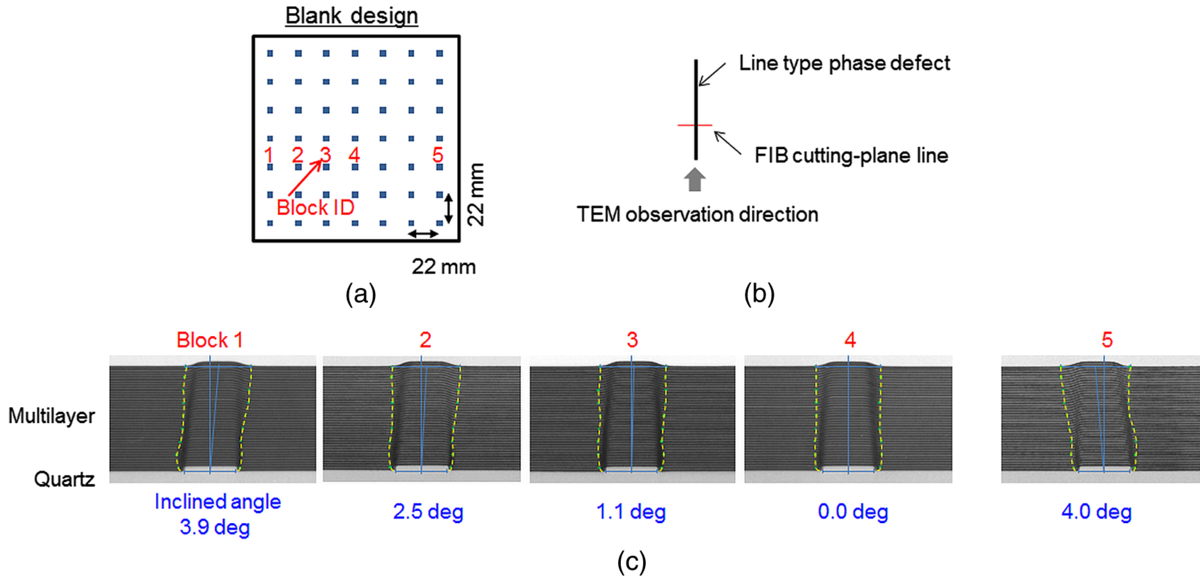

Fig. 4 (a) Arrangement of the test pattern. (b) Direction of the phase defect observation. (c) Cross-sectional TEM images and calculated inclined angles of the phase defects.

determine the angles of the line type phase defects, a set of line type phase defects in blocks 1, 2, 3, 4, and 5 [Fig. 4(a)] were prepared for TEM observation. Figure 4(b) describes the schematic view of the TEM observation direction. Each TEM observation sample was cut perpendicularly to the line type phase defect using a focused ion beam. The TEM images and the inclination angles of the phase defects are shown in Fig. 4(c). The inclination angle was defined as the angle between a vertical line from the quartz substrate surface and a line connecting the center of the line pattern on the quartz substrate with the center of the raised surface of the ML. These TEM images clearly show that the phase defect's propagation through the ML is inclined toward the center of the EUV blank. The relationship between the inclination angles of the phase defects and the distances of the phase defects from the center of the EUV blank is summarized in Fig. 5. Then from this information, the inclination angles of the phase defects in block B [Fig. 1(a)] were estimated to be 4 deg.

3.2 *Measurement of the Phase Defects Using SPM*

The profiles and sizes of the phase defects evaluated in this study were measured using SPM. Figures 6(a) and 6(b) represent the SPM image and cross-sectional profiles of the dot type phase defect on the ML. The measured dimension of the phase defect on the ML was 80.0 nm in full-width at half-maximum and 2.4 nm in height.

The phase defect positions relative to the absorber lines were also measured using SPM. To evaluate the influence of the inclination angles of the phase defects on the EUV microscope images, the same position of the phase defect relative to the absorber line needed to be identified in both block A and block B. Calculating from the total thickness of the ML

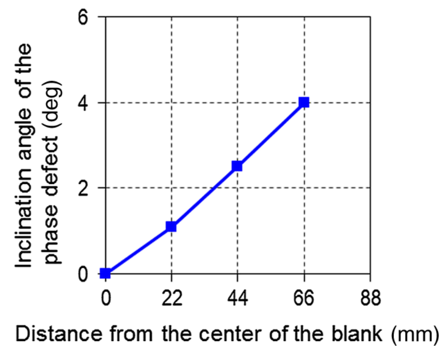

Fig. 5 Inclination angle of the phase defect as a function of the distance of the phase defects from the center of the blank.

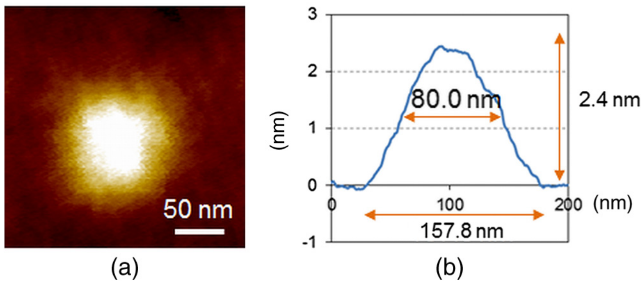

Fig. 6 (a) Scanning probe microscope (SPM) image of the dot type phase defect on the ML. (b) Cross-sectional profile of (a).

and the inclination angle of the phase defect in block B, the phase defect position shifts about 20 nm toward the center of the mask in relation to the position of the dot on the quartz substrate. Figure 7(a) represents a test pattern which, by the help of SPM, enables us to measure the positional shift of the phase defect relative to the absorber pattern. The test pattern consists of a square-shaped absorber hole 1×1 μm in size and a phase defect in the center of the hole. On the mask pattern data, the center of the square hole was aligned with the center of the phase defect. After running through the fabrication process of the programmed phase defect mask, the test patterns in the blocks A and B were measured using SPM. Figure 7(b) shows the cross-sectional profiles of the test pattern in blocks A and B. The measured positional shift of the phase defect in block B was 19.9 nm, which corresponded to 4 deg of the inclination angle. This result agreed well with the result described in Sec. 3.1.

The SPM measurement sites in block B were selected by taking into consideration the positional shift of the phase defects. Figure 8 represents the SPM profiles of the hp 88-nm L/S pattern with dot type phase defect 80 nm in size and 2.4 nm in height prepared for EUV microscope observation. In both blocks A and B, the measured phase defect positions were 0, 8, 56, 88, and 160 nm.

3.3 *Observation of the Phase Defects Using EUV Microscope*

The L/S patterns with various positions of the phase defect shown in Fig. 8 were observed using the EUV microscope.

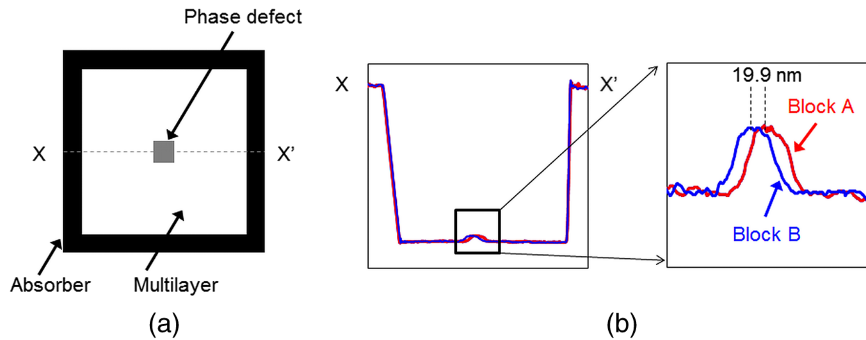

Fig. 7 (a) Design of the test pattern. (b) Cross-sectional profiles along the line X–X′.

Defect position		0 nm	+ 8 nm	+ 56 nm	+ 88 nm	+ 160 nm
Mask design		Absorber Phase defect				
Block A	3-D image					
	Cross sectional view					
Block B	3-D image					
	Cross sectional view					

Fig. 8 SPM images of the programmed phase defect EUV mask and the measured defect positions.

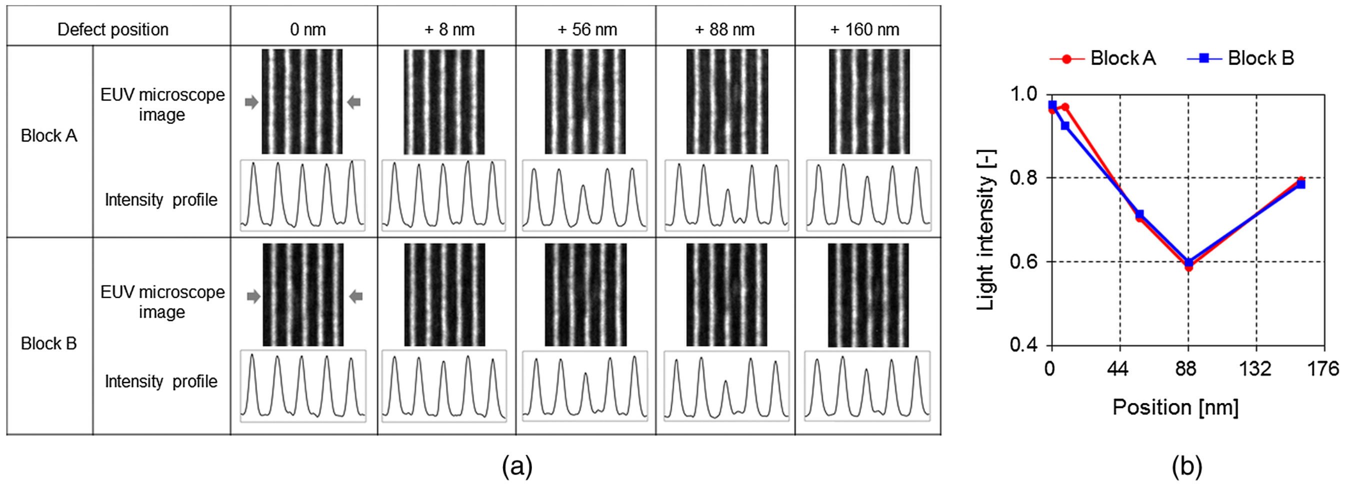

Fig. 9 (a) EUV microscope images and intensity profiles of the programmed phase defect EUV mask. (b) Normalized light intensity of the space pattern image as a function of the defect position.

Figure 9(a) shows the EUV microscope images and their intensity profiles. The intensity fluctuations observed in the images are due to speckle pattern effect occurring with the utilization of a synchrotron EUV source that has a high spatial coherence. These fluctuations are not mask defect.[27] However, the captured images clearly indicate the intensity loss of the EUV light from the space pattern due to the presence of the phase defects. In these cases, the locations of the phase defects were defined as 56, 88, and 160 nm in position. The influence of the phase defect position on the intensity loss of the EUV light was calculated in accordance with Eq. (1). Figure 9(b) represents the normalized light intensity of the space pattern affected by the phase defect as a function of the phase defect position. For both blocks A and B, the maximum drop value of 0.4 was observed at the position of 88 nm; and the intensity differences between blocks A and B were negligibly small at the position of 56 and 160 nm. On the other hand, the impact of the inclination angle on the intensity loss of the EUV light was significant when the phase defect location was 8 nm in position. This phenomenon is the effect of the positional shift of the effective defect position caused by the inclination angle. The effective defect position shifts about 1 nm/ deg to the inclined direction compared with the vertical grown one.[28]

After running through the mask patterning process, removing of the absorber pattern away from the proximity of the phase defect is recommended as an effective way to eliminate the influence of the phase defect on wafer printing image. The decision on the removing area is based on the information of SPM image. However, this study showed that SPM is not a perfect method to pinpoint the actual phase defect position because the phase defect does not always propagate vertically through the ML. On the other hand, a EUV microscope has potential to pinpoint the actual position and affected area by the phase defect.

4 Summary and Conclusion

The fact that a phase defect does not always propagate in a vertical direction from the bottom surface of the ML to the ML's top surface makes it necessary to examine the effect of the phase defect structures on an EUV microscope image of a mask pattern. To prepare the mask with various inclination angles, line patterns were fabricated on the surface of a quartz substrate using a standard mask patterning process. Also, the patterned quartz substrate was then coated with an ML for the purpose of analyzing the phase defect propagation through it. The propagation of the phase defect through the ML was then observed by TEM. An inclination angle of 4 deg was observed at a distance of 66 mm from the center of the EUV blank. Next a programmed dot type phase defect EUV mask was fabricated for the EUV microscope observation. The EUV mask consisted of hp 88-nm L/S patterns, and programmed phase defect 80 nm wide and 2.4 nm high. Finally, the relative positions of the phase defects and absorber patterns were measured by SPM, and an inclination angle dependency of the phase defect impact on the EUV microscope images was clearly observed. The EUV microscope could identify the positional shift of the effective phase defect position caused by the inclined propagation through the ML.

Acknowledgments

The authors are grateful to Tsukasa Abe of Dai Nippon Printing Co., Ltd., for his technical advice, fabrication of the programmed phase defect mask, and measurement of the defect size using SPM. This work was supported by New Energy and Industrial Technology Development Organization (NEDO).

References

1. R. Jonckheere et al., "Dependence of EUV mask printing performance on blank architecture," *Proc. SPIE* **6921**, 69211W (2008).
2. N. Davydova et al, "Mask aspects of EUVL imaging at 27 nm node and below," *Proc. SPIE* **8166**, 816624 (2011).
3. T. Shoki et al., "Improvement of total quality on EUV mask blanks toward volume production," *Proc. SPIE* **7636**, 76360U (2010).
4. H. Kinoshita et al., "Mask technology of extreme-ultraviolet lithography," *Proc. SPIE* **3412**, 358–368 (1998).
5. Y. Arisawa, T. Terasawa, and H. Watanabe, "Impact of EUV mask roughness on lithography performance," *Proc. SPIE* **8679**, 86792S (2013).
6. H. Aoyama et al., "Applicability of extreme ultraviolet lithography to fabrication of half pitch 35 nm interconnects," *Proc. SPIE* **7636**, 76361N (2010).
7. Y. Kikuchi et al., "Study of EUV outgassing spatial distribution toward witness plate in the EUV outgas tester," *Proc. SPIE* **8679**, 86790M (2013).
8. H. Hashimoto et al., "Development of a new mask pattern inspection tool NPI-7000 and applied results to EUV mask inspection," *Proc. SPIE* **8441**, 844117 (2012).

9. R. Hirano et al., "Evaluation of novel projection electron microscopy (PEM) optics for EUV mask inspection," *Proc. SPIE* **8679**, 86791T (2013).
10. S. Shimomura et al., "Demonstration of defect free EUV mask for 22 nm NAND flash contact layer using electron beam inspection system," *Proc. SPIE* **7969**, 79691B (2011).
11. F. Aramaki et al., "Development of new FIB technology for EUVL mask repair," *Proc. SPIE* **7969**, 79691C (2011).
12. M. Waiblinger et al., "e-beam induced EUV photomask repair: a perfect match," *Proc. SPIE* **7545**, 75450P (2010).
13. T. Amano et al., "Study of EUV mask defect repair using FIB method," *Proc. SPIE* **7823**, 782323 (2010).
14. Z. Zhang and T. Liang, "Investigation of resist effects on EUV mask defect printability," *Proc. SPIE* **6730**, 673016 (2007).
15. T. Liang et al., "EUV mask pattern defect printability," *Proc. SPIE* **6283**, 62830K (2006).
16. H. Aoyama et al., "Repair specification study for half-pitch 32-nm patterns for EUVL," *Proc. SPIE* **6730**, 67305L (2007).
17. D. V. den Heuvel et al., "Natural EUV mask blank defects: evidence, timely detection, analysis and outlook," *Proc. SPIE* **7823**, 78231T (2010).
18. T. Onoue et al., "Development of fiducial marks on EUV blanks for defect mitigation process," *Proc. SPIE* **8322**, 832226 (2012).
19. T. Murachi and T. Amano, "Registration accuracy improvement of fiducial mark on EUVL mask with MIRAI EUV ABI prototype," *Proc. SPIE* **8679**, 86791U (2013).
20. T. Murachi, T. Amano, and S. H. Oh, "Fiducial mark requirements from the viewpoints of actinic blank inspection tool for phase-defect mitigation on EUVL mask," *Proc. SPIE* **8522**, 85221U (2012).
21. R. Jonckheere et al., "Repair of natural EUV reticle defects," *Proc. SPIE* **8166**, 81661G (2011).
22. A. Tchikoulaeva et al., "EUV actinic blank inspection: from prototype to production," *Proc. SPIE* **8679**, 86790I (2013).
23. T. Suzuki et al., "EUV actinic blank inspection tool with a high magnification review mode," *Proc. SPIE* **8441**, 844115 (2012).
24. T. Yamane et al., "Phase defect analysis with actinic full-field EUVL mask blank inspection," *Proc. SPIE* **8166**, 81660G (2011).
25. T. Amano, Y. Arisawa, and T. Terasawa, "Impact of the phase defect structure on an actinic dark-field blank inspection signal and wafer printability," *Proc. SPIE* **8322**, 832234 (2012).
26. T. Amano and T. Terasawa, "Propagation of surface topography of EUV blank substrate through multilayer and impact of phase defect structure on wafer image," *Proc. SPIE* **8679**, 86791P (2013).
27. M. Toyoda et al., "At-wavelength extreme ultraviolet lithography mask observation using a high-magnification objective with three multilayer mirrors," *Appl. Phys. Express* **5**(11), 112501 (2012).
28. T. Amano and T. Terasawa, "Propagation of surface topography of extreme ultraviolet blank substrate through multilayer and impact of phase defect structure on wafer image," *J. Micro/Nanolith. MEMS MOEMS.* **12**(3), 033015 (2013).

Tsuyoshi Amano received his BS and MS degrees in applied chemistry from Keio University in 1997 and 1999, respectively. He joined Dai Nippon Printing Co. Ltd., where he carried out research on mask process, metrology, and repair technology. In 2011, he was assigned to EUVL Infrastructure Development Center, Inc. (EIDEC), and since then he has been engaged in the development of patterned masks and blank inspection technology.

Biographies of the other authors are not available.